HHS Public Access

Author manuscript

Psychiatry Res Neuroimaging. Author manuscript; available in PMC 2019 June 30.

Published in final edited form as:

Psychiatry Res Neuroimaging. 2018 June 30; 276: 15–23. doi:10.1016/j.pscychresns.2018.04.002.

Higher 5-HT$_{1A}$ Autoreceptor Binding as an Endophenotype for Major Depressive Disorder Identified in High Risk Offspring. A Pilot Study

Matthew S. Milak[a,d,*], **Spiro P. Pantazatos**[a,d], **Rain Rashid**[a,d], **Francesca Zanderigo**[a,d], **Christine DeLorenzo**[e], **Natalie Hesselgrave**[d], **R. Todd Ogden**[c,d], **Maria A. Oquendo**[e], **Stephanie T. Mulhern**[a,d], **Jeffrey M. Miller**[a,d], **Ainsley K. Burke**[a,d], **Ramin V. Parsey**[f], and **J. John Mann**[a,b,d]

[a]Department of Psychiatry, Columbia University, College of Physicians and Surgeons, New York, New York, United States

[b]Department of Radiology, Columbia University, College of Physicians and Surgeons, New York, New York, United States

[c]Department of Biostatistics, Columbia University, Mailman School of Public Health, New York, New York, United States

[d]Molecular Imaging and Neuropathology Division, New York State Psychiatric Institute, New York, New York, United States

Abstract

Higher serotonin-1A (5-HT$_{1A}$) receptor binding potential (BP$_F$) has been found in major depressive disorder (MDD) during and between major depressive episodes. We investigated whether higher 5-HT$_{1A}$ binding is a biologic trait transmitted to healthy high risk (HR) offspring of MDD probands. Data were collected contemporaneously from: nine HR, 30 depressed not-recently medicated (NRM) MDD, 18 remitted NRM MDD, 51 healthy volunteer (HV) subjects. Subjects underwent positron emission tomography (PET) using [^{11}C]WAY100635 to quantify 5-HT$_{1A}$ BP$_F$, estimated using metabolite, free fraction-corrected arterial input function and cerebellar white matter as reference region. Multivoxel pattern analyses (MVPA) of PET data

*Corresponding author: Matthew S. Milak, M.D., Division of Molecular Imaging and Neuropathology, Department of Psychiatry, College of Physicians and Surgeons, Columbia University, NYSPI Unit 42, New York City, NY 10032, Phone: 646-774-7526, Fax: 646-774-7589, mm2354@cumc.columbia.edu.

[e]Now at Department of Psychiatry, Perelman School of Medicine, Stony Brook, New York, United States

[f]Now at Department of Psychiatry, Stony Brook Medicine, Stony Brook, New York, United States

Conflict of interest

Drs. Milak, DeLorenzo, Ogden, Pantazatos, Parsey, Zanderigo, Ms. Mulhern, Mr. Rashid and Mrs. Hesselgrave report no competing interests. Dr. Burke receives royalties from the Columbia Suicide Severity Rating Scale (C-SSRS). Dr. Oquendo receives royalties for use of the C-SSRS and received financial compensation from Pfizer for the safety evaluation of a clinical facility, unrelated to this pilot study. She has received unrestricted educational grants and/or lecture fees from Astra-Zeneca, Bristol Myers Squibb, Eli Lilly, Janssen, Otsuko, Pfizer, Sanofi-Aventis, and Shire. Her family owns stock in Bristol Myers Squibb. Dr. Mann receives royalties for commercial use of the C-SSRS from the Research Foundation for Mental Hygiene. Dr. Miller's family has owned stock in Johnson & Johnson, unrelated to the current manuscript.

evaluated group status classification of individuals. When tested across 13 regions of interest, an effect of diagnosis is found on BP_F which remains significant after correction for sex, age, injected mass and dose: HR have higher BP_F than HV (84.3% higher in midbrain raphe, 40.8% higher in hippocampus, mean BP_F across all 13 brain regions is 49.9% ± 11.8% higher). Voxel-level BP_F maps distinguish HR *vs.* HV. Elevated 5-HT_{1A} BP_F appears to be a familially transmitted trait abnormality. Future studies are needed to replicate this finding in a larger cohort and demonstrate the link to the familial transmission of mood disorders.

Keywords

major depressive disorder; high risk offspring; positron emission tomography; machine learning; multivoxel pattern analysis; endophenotype; biomarker; 5-HT_{1A} receptor; serotonergic neurotransmission; molecular imaging

1. Introduction

Depressive disorders are estimated to be 40% heritable (Uhl and Grow, 2004), and offspring of individuals with early-onset depression are at higher risk of developing these disorders (Mann et al., 2005). The serotonin (5-HT) system has been implicated in major depressive disorder (MDD) (Blier et al., 1990), and offspring of MDD patients report transient depression after serotonin depletion by acute tryptophan depletion (Klaassen et al., 1999). An endophenotype of MDD may help to identify persons at elevated risk of developing MDD (HR or high risk) while still healthy (no history of a mood disorder). A biomarker or endophenotype could also: (a) improve diagnostic classification by identification of biologic subtypes; (b) improve treatment outcome if biologic subtypes respond to different treatments; (c) guide the search for genetic and environmental factors that mediate the vulnerability to mood disorders and are modifiable to inform a prevention strategy; and (d) help develop and validate animal models of depression.

We have previously reported elevated serotonin-1A (5-HT_{1A}) receptor binding in MDD during a major depressive episode (MDE) across 13 brain regions known to have high 5-HT_{1A} receptor density (Parsey et al., 2010a; Parsey et al., 2006). Most studies (Bhagwagar et al., 2004; Drevets et al., 1999); (Drevets et al., 2007; Sargent et al., 2000; Shively et al., 2006) have not replicated our findings, but we have demonstrated that a key contributor to divergent findings is the choice of outcome measure of binding potential (BP_F, BP_{ND}, or BP_P, as defined using published consensus nomenclature (Innis et al., 2007)) and reference region (RR) (Parsey et al., 2010a). Two studies in depressed humans (N = 16 (Drevets et al., 2007), N = 25 (Sargent et al., 2000)) and one study in depressed non-human primates (N = 17 (Shively et al., 2006)) that showed decreased 5-HT_{1A} receptor binding used BP_{ND} as outcome measure and cerebellum as the RR, including cerebellar gray matter of the vermis, the part of the cerebellum with the highest specific binding which has been shown to influence the direction of the findings (Parsey et al., 2010a). Briefly, when BP_{ND} is used as an outcome measure as opposed to BP_P, it is more likely to find a decrease in BP_{ND} because the total volume of distribution in the RR ($V_{T(RR)}$) of [^{11}C]WAY100635 is less than 1. Since BP_{ND} (but not BP_P) is estimated by dividing by $V_{T(RR)}$, having a fraction in the denominator

makes this formula sensitive to any increase in the estimation of $V_{T(RR)}$ caused by including cerebellar gray matter (which has measurable specific binding) in the delineation of the RR (Hesselgrave and Parsey, 2013; Parsey et al., 2010a; Parsey et al., 2000; Slifstein et al., 2000). One study that used cerebellar white matter as the RR showed decreased BP_P but not BP_{ND} in MDD ($N = 20$ (Hirvonen et al., 2008)).

Higher 5-HT_{1A} receptor binding potential (BP_F) is also present in remitted MDD when between episodes and unmedicated (Miller et al., 2009; Parsey et al., 2010b; Parsey et al., 2006), suggesting that this finding is a biologic trait marker of MDD.

In the current pilot study to determine whether this biologic trait is present in HR subjects prior to developing clinically significant morbidity (and therefore, highly likely to be an endophenotype), we compared 5-HT_{1A} receptor BP_F in HR subjects to that in healthy volunteers (HV), depressed not-recently medicated (NRM) MDD and remitted NRM MDD subjects. We also employed supervised machine learning analyses of our imaging data seeking classification of HR subjects into either MDD or HV groups based on differences between depressed NRM MDD subjects *vs.* HV and remitted NRM MDD subjects *vs.* HV. Clinical follow-up of a subgroup of HR subjects allowed a preliminary comparison of BP_F between those who did and did not subsequently develop MDD (converters *vs.* non-converters or resilient HR subjects).

2. Methods and materials

2.1. Subjects

Data from nine HR, 30 unrelated depressed NRM MDD, 18 unrelated remitted NRM MDD subjects, and 51 HV were analyzed for this pilot study. The data from HV and all NRM MDD subjects are presented for comparison purposes but were previously published (Kaufman et al., 2015; Parsey et al., 2010a). The HR sample was recruited and their PET data were acquired contemporaneously with the comparison groups: HV, depressed NRM MDD, and remitted NRM MDD. Subjects were recruited through print and online advertisements and referral from our clinical populations.

Subjects were classified as HR if they had no lifetime or current history of a DSM-IV psychiatric illness based on a structured clinical interview (SCID I) (First et al., 1995) and had one or more first-degree relatives with a history of early-onset (< 30 years of age) MDD. Five subjects reported having one first-degree relative with a history of MDD (a parent in all cases), and four reported having two or more (i.e., at least one parent and a sibling). No subject confirmed a history of depression in both parents. All subjects provided consent for the Principal Investigator to contact their relative(s) with a history of MDD to confirm their reports. Research interviews were conducted by clinical raters holding Master's degrees or higher. Assessment instruments used for ascertaining family history of mood disorders included a baseline demographic interview, the Childhood Experiences Questionnaire (CEQ)-Modified Abuse History, the Family History for Genetic Studies (FIGS), and the Parental Bonding Instrument (PBI).

Additional inclusion criteria included: age between 18 to 32 years, absence of history of treatment with psychotropic medication, taking no other medications impacting the serotonin system for a minimum of 6 months or any anticoagulant medication for a minimum of 10 days. Exclusion criteria consisted of: current or past MDE or other Axis I psychiatric diagnosis, current or past alcohol or drug use disorder, history of IV drug use or ecstasy use more than twice, family history of schizophrenia, significant active physical illness, lacking capacity to consent, pregnancy, presence of metal implants or a medicinal patch, medical or occupational radiation exposure within the past 12 months, or a head injury causing loss of consciousness for more than three minutes. New York State Psychiatric Institute/Columbia Institutional Review Board-approved written informed consent was obtained from all subjects after they were given a description of the study.

2.2. Radiochemistry and input function measurement

Preparation of [^{11}C]WAY100635 was performed as previously described (Parsey et al., 2000). Between 96.2 and 732.6 MBq of [^{11}C]WAY100635 were injected (Supplementary Table 1). Mean injected mass (μg) differed across groups ($F = 9.00$, $df = 2, 87$, $p < 0.001$); a pairwise post hoc test revealed that the HV group received higher mass than the depressed NRM MDD and HR groups, which received comparable mass. Though we have shown that injected mass in this range does not correlate with binding potential (Miller et al., 2009), we adjusted for injected mass in the analyses.

Arterial plasma radioactivity, metabolites, and plasma free fraction (f_P) were collected and assayed as previously described (Parsey et al., 2006; Parsey et al., 2000). Unmetabolized parent fraction levels were fit with a Hill function (Wu et al., 2007). The input function was corrected for unmetabolized tracer by multiplying the total plasma counts with the interpolated parent fraction. The metabolite-corrected arterial input function was fit as the combination of a straight line and the sum of three decreasing exponentials, describing the function before and after the peak, respectively.

2.3. Image acquisition and analysis

PET image acquisition protocol details have been previously described (Parsey et al., 2010a; Parsey et al., 2006; Parsey et al., 2000). Briefly, venous and arterial catheters were used to inject radiotracer and to obtain arterial samples for the input function, respectively. The head was immobilized using a polyurethane head holder system (Soule Medical; Tampa, FL, USA). PET imaging was performed using an ECAT Exact HR+ (Siemens/CTI; Knoxville, TN, USA). Data were collected in 3D mode for 110 minutes in 20 frames of increasing duration: 3 at 20 seconds, 3 at 1 minute, 3 at 2 minutes, 2 at 5 minutes and 9 at 10 minutes.

Images were reconstructed, using attenuation correction from the transmission data, to a 128 × 128 matrix (pixel size: 1.72 × 1.72 mm). A model-based method was used to correct scatter (CC et al., 1996). A Shepp filter of 0.5 (2.5 mm in full width at half maximum, FWHM) was used for the reconstruction and estimated image. The Z filter was all-pass 0.4 (2.0 mm in FWHM), and the zoom factor was 4.0, leading to a final image resolution of 5.1 mm at FWHM at the center of the field of view (Mawlawi et al., 2001).

The last 12 frames of each pilot study were registered to the eighth frame using the FMRIB linear image registration tool (FLIRT) version 5.0 (FMRIB Image Analysis Group, Oxford, UK). Linear co-registration was performed between the averaged motion-corrected PET frames and the MRI as previously described (DeLorenzo et al., 2009).

Acquisition of T1-weighted MRI images for co-registration of PET images and identification of regions of interest (ROIs) was performed as previously described using a 3T Signa HDx system (General Electric Medical Systems; Milwaukee, WI, USA) (Milak et al., 2010). Regional delineations were obtained automatically for all ROIs except for dorsal raphe nucleus (RN), which was manually located on each PET image and delineated by a fixed-volume (20 mm^3) elliptical ROI (Parsey et al., 2010a; Parsey et al., 2006). Automatic ROIs were obtained using nonlinear registration techniques to warp 18 manually outlined MRIs. The 18 templates were registered to the skull-stripped (using Atropos, (Avants et al., 2011)) target brain MRI using the Automatic Registration Toolbox (ART (Ardekani et al., 2005)), which was a top performer in an evaluation of 14 nonlinear brain registration algorithms (Klein et al., 2009). The probabilistic regional label for each target voxel was then determined by evaluating the percentage of the 18 normalized brains assigning that regional label to the voxel. For cortical regions, this probability was multiplied by the probability of the voxel being in the gray matter, as determined by SPM5 (Wellcome Trust Centre for Neuroimaging, London, UK). The labels are therefore probabilistic and these probabilities are used in the calculation of the time–activity curves (TACs). MRI-based ROIs were applied to each frame of the PET images using the co-registration transformation. TACs were then generated by averaging the measured activity within a region over the time course of the PET acquisition.

The PET outcome measure of interest used in this study and most closely reflecting the density of available receptors *in vivo* (B_{avail}) is BP_F (= B_{avail}/K_D, where K_D is the equilibrium dissociation constant) (Gunn et al., 1998; Innis et al., 2007). A full description of the modeling approach used to quantify BP_F may be found elsewhere (Parsey et al., 2010a; Parsey et al., 2001). Briefly, at the ROI level, we fitted the TACs using a constrained kinetic two-tissue compartment model (i.e., constraining the non-displaceable binding in each target region to be equal to the tracer distribution volume in the RR (Parsey et al., 2000)). The cerebellar white matter (CWM) RR was selected because it has the least specific binding of all available options and was fitted with a one-tissue compartment model (Parsey et al., 2005). BP_F was calculated as $(V_{T(ROI)}–V_{T(RR)})/f_P$, where V_T is the total volume of distribution in the specified region.

At the voxel level, BP_F was estimated using the basis pursuit strategy (Gunn et al., 2002), which provides parametric images from dynamic radiotracer data without the need to specify a compartmental structure. Briefly, this data-driven approach is based on the general compartmental theory for description of the radiotracer's kinetics and determines a parsimonious model consistent with the measured data. This approach uses basis pursuit denoising, a technique that involves the determination of a sparse selection of kinetic basis functions from an over-complete dictionary to compromise between the error in the description of the measured data and the sparseness of the representation. This approach provides estimates of the system's macro parameters (i.e., V_T) and the corresponding

number of numerically identifiable compartments in the system. This approach determines the most appropriate model from the information contained within the measured data and requires no *a priori* knowledge of the radiotracer kinetics, besides the choice of the family of basis functions that constitutes the dictionary, which needs to be in a range physiologically plausible for the considered radiotracer. Here, we used a range spaced in a logarithmic manner to elicit a suitable coverage of the kinetic spectrum, as suggested for the radiotracer [^{11}C]WAY100635 (Gunn et al., 2002). Once the V_T parametric images were obtained in each subject using the basis pursuit strategy, the corresponding BP_F images were generated by subtracting in each voxel the V_T of the CWM—validated as RR for [^{11}C]WAY100635 (Parsey et al., 2000)—and dividing by f_P. All methods were implemented in MATLAB (R2009b, The MathWorks, Natick, MA).

2.4. ROI-based statistical analyses

Statistical analyses were performed in R 3.1.2 (http://cran.r-project.org). Linear mixed effects models incorporated outcome measure data from all ROIs simultaneously, with ROI as the fixed effect and subject and date of experiment as the random effects. By considering all ROIs simultaneously, we gain statistical power and avoid the issues of multiple comparisons. Covariates were included as fixed effects as needed.

The validity of classical inferential statistics such as analysis of variance (e.g., with a mixed effects model) is contingent upon the data tested fulfilling all the assumptions of the test applied (i.e., normality of distribution, compound symmetry, sphericity, kurtosis) (Carlson et al., 2013; Dunn and Clark, 1987; Pantazatos et al., 2012). Power transformations are a set of mathematical data transformations that are applied based on the findings of the residual analysis to transform the data so that it fulfills the assumptions mentioned above. Log transformation of the imaging data yielded normal distribution meeting the requirements for the analysis of variance.

Additionally, bootstrap errors were calculated for each subject for every ROI observation that took into account the error in modeling the metabolite, plasma, and TACs (Ogden and Tarpey, 2006). All observations were weighted according to the calculated bootstrap error.

Additional statistical analyses performed include Student's *t*-test, Fisher's exact test, and chi-squared tests performed in SPSS 19.0 (IBM, SPSS Statistics, 2011).

2.5. Voxel-based univariate analyses and multivariate machine learning-based analyses

Voxel-level analyses were conducted to validate ROI findings and to explore brain-wide for other regions of difference. Voxel-level PET (BP_F) maps were spatially normalized using ART and interpolated to 2 × 2 × 2 mm voxel resolution, smoothed with an 8 mm Gaussian kernel, and submitted to a 1-way ANCOVA with three levels: HV, $N = 51$; depressed NRM MDD, $N = 29$; HR, $N = 9$ (due to excessive cropping and difficulties in spatial normalization, 1 depressed NRM MDD subject who was included in the above ROI analyses was dropped from subsequent voxel-based analyses). An absolute threshold was applied to remove voxels with BP_F values below 5, and non-gray matter voxels were excluded from analyses via a gray matter mask generated by thresholding a tissue probability map in MNI space (provided with SPM8) at > 0.2. Covariates were entered stepwise and non-significant

covariates were removed. Sex was included as a nuisance covariate, and these effects were removed from features (voxel BP_F values) prior to classification analyses using multivoxel pattern analysis (MVPA, see below). Analyses were conducted using SPM8 (www.fil.ion.ucl.ac.uk/spm/) and implemented in MATLAB version 7.13 on Ubuntu Linux OS 12.0.4.

MVPA analyzes the joint BP_F signal across multiple regions in a single subject in order to predict the diagnostic class of that subject. There is no direction associated with the predictions (i.e., class labels are arbitrarily positive or negative). To make MVPA computationally tractable and reduce dimensionality, PET maps were resampled from 2 × 2 × 2 mm voxel resolution to 6 × 6 × 6 mm resolution. For all binary classification tasks, a linear kernel Support Vector Machine SVM (Vapnik, 1999) with a filter feature selection (*t*-test) and leave-one-out cross-validation was applied using the Spider v1.71 MATLAB toolbox (http://people.kyb.tuebingen.mpg.de/spider/) with default regularization parameter $C = 1$. During each iteration of leave-one-out cross-validation, one subject was withheld from the data set and: (a) a 2-sample *t*-test was performed over the remaining training data; (b) the features were ranked by absolute *t*-score and the top 25, 50, 75…to 500 features were selected; (c) these selected features were then used to predict the class of the withheld test examples during the classification stage. Classification performance is reported in terms of "area under the curve" (AUC), i.e., area under the receiver operator characteristic (ROC) curve (Hanley and McNeil, 1982), which is the arithmetic mean of sensitivity (true positive rate) and specificity (true negative rate). Significance was assessed using permutation as in Golland and Fischl (2003). *P*-values for the peak AUC values were calculated with respect to the 4,000 null values obtained above, and corrected *p*-values were obtained by Bonferroni correction for the number of comparisons (in this case 20, corresponding to the top 25, 50, 75…500 selected features). We note that this approach (plotting performance *vs.* number of selected features) is not biased, since for each top selected number of features, and for each round of leave-one-out cross validation, the features were selected from a training set (i.e., total number of samples minus one) that was completely independent from the testing set (i.e., one left out sample). We also conducted analyses whereby models trained to discriminate depressed NRM MDD *vs.* HV and remitted NRM MDD *vs.* HV were applied to HR subjects and compared to follow-up data (i.e., were MDD converters classified as MDD or HV?). For display purposes, the top 75 features in classifying HR *vs.* HV were selected from and used to train a model over the entire dataset in order to estimate and display their SVM weights on the brain.

2.6. Diagnostic follow-up

The first author completed follow-up during two weeks five to seven years after the PET scan acquisition on five out of nine HR subjects who were reachable for a semi-structured interview (Zimmerman, 1994). Occurrence of a MDE since PET scan acquisition was determined by patient-reported history and treatment and confirmed by the semi-structured interview.

3. Results

3.1. Demographic and clinical results

HR subjects do not differ from HV in sex ratio ($p = 0.94$) or lifetime aggression severity ($p = 0.68$) but are younger because we deliberately recruited younger subjects who had not passed the age of risk ($p = 0.02$; Table 1). Similarly, HR subjects show no differences from the depressed NRM MDD group in sex ratio ($p = 0.27$) and lifetime aggression severity ($p = 0.10$) but are younger than the depressed NRM MDD group ($p = 0.002$). The Hamilton Depression Rating Scale (HDRS) scores of the HR subjects are lower than those of the depressed NRM MDD group ($p < 0.001$) and slightly higher than those of HV ($p = 0.006$), but still within normal range.

3.2. ROI-based 5-HT$_{1A}$ binding potential (BP$_F$) results

A main effect of diagnosis is found for BP_F tested simultaneously across all 13 ROIs between HV, HR, and depressed NRM MDD subjects ($F = 11.54$, $df = 2, 87$, $p < 0.0001$; Figure 1 and Supplementary Figure 1). This finding is preserved when corrected for sex, age, injected mass, and tracer dose ($F = 8.1$, $df = 2, 83$, $p = 0.0006$). Post hoc testing shows that the HR group has higher BP_F compared with HV ($F = 8.69$, $df = 1, 87$, $p = 0.004$; Figure 1 and Supplementary Figure 1) but does not differ from the depressed NRM MDD group ($F = 0.021$, $df = 1, 87$, $p = 0.884$). Average BP_F in HR subjects is 49.9% ± 11.8% higher than that in HV and comparable to that in depressed NRM MDD subjects. There is no difference in binding between HR subjects with one first-degree relative with a history of MDD *vs.* those with two or more such relatives. Confirming that the reference region difference does not account for the findings, an ANOVA to evaluate the main effect of diagnosis on $V_{T(RR)}$ shows that $V_{T(RR)}$ does not differ across groups ($F = 0.093$, $df = 2, 86$, $p = 0.911$).

3.3. Voxel-based 5-HT$_{1A}$ binding potential (BP$_F$) results

Voxel-based analysis shows an effect of diagnosis on 5-HT_{1A} BP_F between HV, HR, and depressed NRM MDD subjects (correlation between ROI- and voxel-based results: $R^2 = 0.911$; slope = 0.865, Figure 2, left side, Supplementary Table 2). BP_F in HR and depressed NRM MDD subjects *vs.* HV is highest in midbrain, parahippocampal gyrus, and ventral prefrontal cortex (Figure 2, right side).

MVPA shows that voxel-based 5-HT_{1A} BP_F maps contain sufficient information to distinguish HR *vs.* HV with well above chance performance (even after correcting for sex; mean AUC = 0.80, $p < 0.005$, Figure 3A, Table 2). The highest discrimination is obtained between HR *vs.* HV using the top 75 selected features (peak AUC = 0.87, $p < 0.0005$, sensitivity = 0.78, specificity = 0.96). The results suggest depressed NRM MDD subjects are weakly distinguishable from HV at 25 features (AUC = 0.62, $p = 0.08$), but at > 25 features, even though the AUC remains above 0.5 (theoretical chance level) across all top N selected features, it is not significant ($p = 0.17$). The HR subjects are indistinguishable from depressed NRM MDD subjects across all features (mean AUC = 0.49, $p = 0.43$). High HR *vs.* HV classification accuracy remains after correcting for age and sex (i.e., after removing the variance explained by age and sex) (mean AUC = 0.72, $p < 0.005$, peak AUC = 0.81, $p =$

0.00025, data not shown), as well as after correcting for age, sex, and injected mass (mean AUC = 0.62, $p = 0.03$, peak AUC = 0.80, $p = 0.00025$). Informative voxels discriminating HR *vs.* HV are displayed in Figure 3B. Repeating the MVPA using a balanced sub-sample of HV and depressed NRM MDD subjects matched for age and sex ($N = 9$ each group) shows that HR remain distinguishable from HV (mean AUC = 0.69, $p = 0.03$; Supplementary Figure 2) and indistinguishable from depressed NRM MDD subjects (mean AUC = 0.55, $p = 0.27$), and HV are distinguishable from depressed NRM MDD subjects (mean AUC = 0.77, $p = 0.02$) (data not shown).

Owing to the relatively low classification rates of HV *vs.* depressed NRM MDD groups (when using the full depressed NRM MDD dataset), we conducted an additional MVPA analysis of HV *vs.* an independent group of remitted NRM MDD subjects ($N = 18$, mean (SD) age = 34.8 (12.7), 13 females) under the assumption that the remitted NRM MDD subjects would be more similar to non-depressed HR subjects and also have less globally correlated BP_F (which could influence MVPA performance, see Discussion). We find that MVPA performance is higher when classifying remitted NRM MDD *vs.* HV, controlling for sex (peak balanced accuracy = 0.78, sensitivity = 0.67, specificity = 0.9, $p < 0.05$ corrected, data not shown).

3.4. Diagnostic follow-up

Two of the five HR subjects report a MDE since the PET scan to date. These subjects have the highest raphe midbrain binding of the five subjects for whom we have follow-up clinical data (Figure 4). The converters and non-converters cleanly separate on BP_F in most ROIs, and the overall group has an indication of a bimodal distribution consistent with a subgroup having the biologic risk trait.

We also compared the predictions of a HV *vs.* depressed NRM MDD discriminative model applied to the HR subjects with our follow-up data in 5 of the 9 HR subjects. We hypothesized that the model would classify MDD converters as MDD and the non-converters as HV. We find that both MDD converters are classified as MDD, whereas one of three non-converters is classified as HV (the same is found when applying a model trained to discriminate HV *vs.* remitted NRM MDD subjects).

4. Discussion

This pilot study provides novel evidence in support of a particular pattern of elevated 5-HT_{1A} binding in midbrain dorsal raphe nuclei and serotonergic terminal fields representing an endophenotype (a special type of biomarker), implying familial transmission of MDD. Shields and Gottesman's operational requirements (Peterson and Weissman, 2011) for a biomarker to be an endophenotype are that it: (a) is associated with the illness in the general population; (b) is heritable; (c) is a trait (i.e., present in an affected individual whether or not the illness is active); (d) co-segregates with illness within the affected families; and (e) is found in non-affected family members at a higher rate than in the general population (Leboyer et al., 1998). Our previously published findings support criteria (a) and (c) by demonstrating elevated 5-HT_{1A} binding in MDD during a MDE (Parsey et al., 2010a; Parsey et al., 2006) and between MDEs in remitted, unmedicated MDD (Miller et al., 2009). Here

we report novel evidence for criterion (e), by demonstrating elevated 5-HT_{1A} binding in healthy members of affected families, criterion (c), by demonstrating the presence of this biomarker in these HR subjects who have later gone on to develop MDD, and indirect support for criterion (b). The follow-up data in a subgroup of HR subjects are consistent with the hypothesis that higher 5-HT_{1A} binding confers elevated risk of developing MDD in HR subjects.

The cause of this higher binding is uncertain, but serotonin neuron cell cultures, though not non-serotonin hippocampal target neuron cultures (Albert and Lemonde, 2004), show higher expression by the G allele in a C(-1019)G promoter polymorphism (Parsey et al., 2010a; Parsey et al., 2006). In raphe serotonergic neuron cell cultures, the G allele does not bind the nuclear deformed epidermal autoregulatory factor (NUDR) transcriptional repressor, resulting in elevated expression of the 5-HT_{1A} autoreceptor in the RN (Czesak et al., 2006; Lemonde et al., 2003). This is not the case for non-serotonergic neurons such as hippocampal target neurons with 5-HT_{1A} receptors on their membranes. We and others (Lemonde et al., 2003) report an association between the C(-1019)G functional polymorphism of the promoter region of the 5-HT_{1A} gene and MDD and bipolar depression. These findings led us (Parsey et al., 2006) and others (Albert and Lemonde, 2004; Lemonde et al., 2003) to propose a model of depression based on over-expression of the 5-HT_{1A} autoreceptor in MDD. This over-expression of 5-HT_{1A} somatodendritic autoreceptors results in reduced serotonin neuron firing and reduced serotonin release (Richardson-Jones et al., 2010). Although our sample size of HR offspring was too small to detect such a genetic effect, we have previously reported such a relationship in both MDD and bipolar disorder (Parsey et al., 2006; Sullivan et al., 2009). C(-1019)G functional polymorphism of the promoter region of the 5-HT_{1A} gene does not explain upregulation of terminal field postsynaptic 5-HT_{1A} receptors (Parsey et al., 2010a; Parsey et al., 2006), which is more likely a result of homeostatic upregulation, secondary to reduced intrasynaptic serotonin release (Compan et al., 1998).

The age difference between groups, as well as a difference in injected mass between groups (Supplementary Table 1), does not explain the findings (i.e., neither age nor injected mass is correlated with BP_F), and group differences remain when including age, injected mass, and/or tracer dose as nuisance covariates in the model. Although the difference in f_P between HR and HV groups does not reach significance in the current cohort ($p = 0.059$, Supplementary Figure 3), we have previously shown that even in cohorts in which f_P is different between groups, this difference does not drive the primary finding of elevated 5-HT_{1A} binding in MDD (Parsey et al., 2010a). In the current cohort, we find higher binding in HR *vs.* HV whether we use BP_F (Figure 1) or BP_P ($p < 0.001$), the latter of which does not require measurement of f_P ($BP_P = f_P \times B_{avail}/K_D$) (Gunn et al., 1998; Innis et al., 2007). It is unlikely that these findings are an artifact of a partial volume effect because we detected an effect of diagnosis on BP_F in both small regions (such as raphe nuclei and insula) and large regions (such as parietal and occipital cortices). A partial volume effect would have led to underestimation of BP_F in the diagnostic group that may have had smaller raphe nuclei, such as the MDD group, but the direction of the findings is in the opposite direction to that potentially attributable to a partial volume effect, namely, depressed NRM MDD subjects have higher BP_F than HV.

The results of our preliminary study suggest that the particular pattern of elevated 5-HT_{1A} binding reported here may be an endophenotype that distinguishes HR subjects truly at elevated risk for developing MDD from other offspring of early-onset MDD patients (presumably non-carriers of a genetic constellation and/or its interactions with environment that may contribute to the risk of developing MDD). Familial transmission implies that not all offspring of MDD probands should manifest an elevation in 5-HT_{1A} binding and predicts a bimodal distribution of BP_F in HR subjects. Our MVPA results are consistent with this hypothesis in that just over half of the HR subjects are classified as HV. We do not observe high discrimination between depressed NRM MDD subjects *vs.* HV: counterintuitively, HV are more distinguishable from HR subjects than they are from depressed NRM MDD subjects. Perhaps in currently depressed subjects, BP_F is more spatially correlated (i.e., there is a homogenous increase in BP_F) and hence there is less information content to be leveraged by MVPA. The higher MVPA performance when classifying remitted NRM MDD *vs.* HV is consistent with this hypothesis.

The follow-up data, although preliminary, are promising. Two out of the five subjects who were reachable for a diagnostic interview developed clinical depression, were diagnosed with MDD, and treated successfully with antidepressants. At the time of the follow-up interview, both converters were in full sustained remission. A MVPA model trained to discriminate HV *vs.* depressed NRM MDD subjects classifies both converters as MDD, and one of three non-converters is classified as HV. This is consistent with the hypothesis that the pattern of elevated BP_F is an endophenotype for MDD and that MVPA of BP_F patterns can potentially be used to predict risk for development of MDD in HR subjects. If these data are replicated in independent samples, then the particular pattern of elevated BP_F identified here may be further refined and confirmed as an endophenotype for MDD. This potential for detecting subjects most likely to convert may open the door for research into preventive interventions (such as psychological and pharmacological interventions to increase resilience and improve stress tolerance) to attempt to prevent development of MDD in these individuals. It is important to recognize, however, that depression is likely not monolithic in its etiology. Therefore, identification of additional biomarkers (endophenotypes) may improve detection of risk in HR individuals that are likely to convert to MDD.

Limitations

BP_F is highly sensitive to measurement error in the free fraction (f_p) and this error potentially limits detection of differences in mean BP_F. We used an external standard to reduce assay variance and the larger variance of f_p in HV *vs.* HR (2.4% *vs.* 1.6%) does not prevent detection of group difference in BP_F. We find no group differences in $V_{T(RR)}$ indicating that the reference region does not account for the main findings. Although one of the MDD converters shows unexpectedly low BP_F in one of the smallest ROIs (raphe nuclei), PET quantification of BP_F in smaller volume regions is particularly prone to measurement error, yet our findings are the same at a group level across all ROIs (see the linear mixed effects model in the Methods section).

The generalizability of this pilot study's findings is limited primarily because of the small sample size of the HR group (see section entitled "Supplementary Material for HR Sample

Size"), which could not be expanded because use of [^{11}C]WAY100635 has been curtailed due to the technical difficulties of the Grignard reaction. Leave-one-out cross validation (LOOCV) has more variance (*vs.* K-fold cross validation) in mean accuracy across datasets (owing to higher dependency in results across trainings folds). However, it was the best cross validation option given the limited sample size in order to provide sufficient training data while testing accuracy of the model in an unbiased way. In support of our conclusion, HR subjects are still distinguishable from HV after correcting for potential confounds such as age, sex, and injected mass. Given the small sample size of the HR group, MVPA results of this study should also be considered preliminary until replicated in independent samples. The small HR group sample size needs to be increased to identify subgroups (i.e., susceptible *vs.* resilient) for future prospective studies.

Conclusion

These preliminary data suggest that elevated 5-HT$_{1A}$ binding found in HR subjects is an endophenotype by providing evidence that this biomarker is present in healthy, not (yet) affected offspring of MDD probands. In addition, the data obtained by longitudinal follow-up (five plus years) suggest that those with the highest binding convert to MDD. Future studies should focus on replicating this finding in larger samples of HR subjects as identification of HR subjects, and consequently the development of preventive interventions in HR subjects, is a major unmet challenge in psychiatry. If autoreceptor binding reflects relative risk, consideration should be given to preventive intervention trials in HR subjects (with this endophenotype), with pharmacological agents known to down-regulate 5-HT$_{1A}$ autoreceptors (i.e., selective serotonin reuptake inhibitors) (Gray et al., 2013).

Supplementary Material

Refer to Web version on PubMed Central for supplementary material.

Acknowledgments

Binod Thapa Chhetry assisted in WAY voxel-based analyses. Harry Rubin-Falcone assisted with data analysis and presentation. Support was provided by the NARSAD Young Investigator Award of 2004—(9170)MSM, NIMH grant MH040695 (JJM), a Paul Janssen Translational Neuroscience Postdoctoral Research Fellowship (SPP), and NIMH grant MH108721 (SPP).

References

Albert PR, Lemonde S. 5-HT1A receptors, gene repression, and depression: guilt by association. The Neuroscientist: a review journal bringing neurobiology, neurology and psychiatry. 2004; 10:575–593.

Ardekani BA, Guckemus S, Bachman A, Hoptman MJ, Wojtaszek M, Nierenberg J. Quantitative comparison of algorithms for inter-subject registration of 3D volumetric brain MRI scans. J Neurosci Methods. 2005; 142:67–76. [PubMed: 15652618]

Avants BB, Tustison NJ, Wu J, Cook PA, Gee JC. An open source multivariate framework for n-tissue segmentation with evaluation on public data. Neuroinformatics. 2011; 9:381–400. [PubMed: 21373993]

Bhagwagar Z, Rabiner EA, Sargent PA, Grasby PM, Cowen PJ. Persistent reduction in brain serotonin1A receptor binding in recovered depressed men measured by positron emission tomography with [11C]WAY-100635. Molecular psychiatry. 2004; 9:386–392. [PubMed: 15042104]

Blier P, de Montigny C, Chaput Y. A role for the serotonin system in the mechanism of action of antidepressant treatments: preclinical evidence. The Journal of clinical psychiatry. 1990; 51(Suppl): 14–20. discussion 21.

Carlson PJ, Diazgranados N, Nugent AC, Ibrahim L, Luckenbaugh DA, Brutsche N, Herscovitch P, Manji HK, Zarate CA Jr, Drevets WC. Neural correlates of rapid antidepressant response to ketamine in treatment-resistant unipolar depression: a preliminary positron emission tomography study. Biological psychiatry. 2013; 73:1213–1221. [PubMed: 23540908]

CCW, DN, MEC. A Single Scatter Simulation Technique fo Scatter Correction in 3D PET. In: Grangeat, P., Amans, J-L., editors. Three-dimensional image reconstruction in radiology and nuclear medicine. Kluwer Academic Publishers; Dordrecht; Boston: 1996. p. 255-268.

Compan V, Segu L, Buhot MC, Daszuta A. Differential effects of serotonin (5-HT) lesions and synthesis blockade on neuropeptide-Y immunoreactivity and 5-HT1A, 5-HT1B/1D and 5-HT2A/2C receptor binding sites in the rat cerebral cortex. Brain research. 1998; 795:264–276. [PubMed: 9622647]

Czesak M, Lemonde S, Peterson EA, Rogaeva A, Albert PR. Cell-specific repressor or enhancer activities of Deaf-1 at a serotonin 1A receptor gene polymorphism. J Neurosci. 2006; 26:1864–1871. [PubMed: 16467535]

DeLorenzo, C., Klein, A., Mikhno, A., Gray, N., Zanderigo, F., Mann, JJ., Parsey, RV. A new method for assessing PET-MRI coregistration. SPIE Medical Imaging; Florida, USA. 2009. 72592W-72592W-72598

Drevets WC, Frank E, Price JC, Kupfer DJ, Holt D, Greer PJ, Huang Y, Gautier C, Mathis C. PET imaging of serotonin 1A receptor binding in depression. Biological psychiatry. 1999; 46:1375–1387. [PubMed: 10578452]

Drevets WC, Thase ME, Moses-Kolko EL, Price J, Frank E, Kupfer DJ, Mathis C. Serotonin-1A receptor imaging in recurrent depression: replication and literature review. Nuclear medicine and biology. 2007; 34:865–877. [PubMed: 17921037]

Dunn, OJ., Clark, V. Applied probability and statistics. 2. Wiley; New York: 1987. Applied statistics: analysis of variance and regression, Wiley series in probability and mathematical statistics; p. xiip. 445

First, M., Spitzer, R., Gibbon, M., Williams, J. Structured Clinical Interview for DSM-IV Axis I Disorders (SCID-I/P, Version 2.0). Biometrics Research Dept., New York State Psychiatric Institute; New York: 1995.

Golland P, Fischl B. Permutation tests for classification: towards statistical significance in image-based studies. Inf Process Med Imaging. 2003; 18:330–341. [PubMed: 15344469]

Gray NA, Milak MS, DeLorenzo C, Ogden RT, Huang YY, Mann JJ, Parsey RV. Antidepressant treatment reduces serotonin-1A autoreceptor binding in major depressive disorder. Biological psychiatry. 2013; 74:26–31. [PubMed: 23374637]

Gunn RN, Gunn SR, Turkheimer FE, Aston JA, Cunningham VJ. Positron emission tomography compartmental models: a basis pursuit strategy for kinetic modeling. Journal of cerebral blood flow and metabolism: official journal of the International Society of Cerebral Blood Flow and Metabolism. 2002; 22:1425–1439.

Gunn RN, Sargent PA, Bench CJ, Rabiner EA, Osman S, Pike VW, Hume SP, Grasby PM, Lammertsma AA. Tracer kinetic modeling of the 5-HT1A receptor ligand [carbonyl-11C]WAY-100635 for PET. NeuroImage. 1998; 8:426–440. [PubMed: 9811559]

Hanley JA, McNeil BJ. The meaning and use of the area under a receiver operating characteristic (ROC) curve. Radiology. 1982; 143:29–36. [PubMed: 7063747]

Hesselgrave N, Parsey RV. Imaging the serotonin 1A receptor using [11C]WAY100635 in healthy controls and major depression. Philosophical transactions of the Royal Society of London. Series B, Biological sciences. 2013; 368:20120004. [PubMed: 23440462]

Hirvonen J, Karlsson H, Kajander J, Lepola A, Markkula J, Rasi-Hakala H, Nagren K, Salminen JK, Hietala J. Decreased brain serotonin 5-HT1A receptor availability in medication-naive patients with major depressive disorder: an in-vivo imaging study using PET and [carbonyl-11C]WAY-100635. Int J Neuropsychopharmacol. 2008; 11:465–476. [PubMed: 17971260]

Innis RB, Cunningham VJ, Delforge J, Fujita M, Gjedde A, Gunn RN, Holden J, Houle S, Huang SC, Ichise M, Iida H, Ito H, Kimura Y, Koeppe RA, Knudsen GM, Knuuti J, Lammertsma AA, Laruelle M, Logan J, Maguire RP, Mintun MA, Morris ED, Parsey R, Price JC, Slifstein M, Sossi V, Suhara T, Votaw JR, Wong DF, Carson RE. Consensus nomenclature for in vivo imaging of reversibly binding radioligands. Journal of cerebral blood flow and metabolism: official journal of the International Society of Cerebral Blood Flow and Metabolism. 2007; 27:1533–1539.

Kaufman J, Sullivan GM, Yang J, Ogden RT, Miller JM, Oquendo MA, Mann JJ, Parsey RV, DeLorenzo C. Quantification of the Serotonin 1A Receptor Using PET: Identification of a Potential Biomarker of Major Depression in Males. Neuropsychopharmacology: official publication of the American College of Neuropsychopharmacology. 2015

Klaassen T, Riedel WJ, van Someren A, Deutz NE, Honig A, van Praag HM. Mood effects of 24-hour tryptophan depletion in healthy first-degree relatives of patients with affective disorders. Biol Psychiatry. 1999; 46:489–497. [PubMed: 10459398]

Klein A, Andersson J, Ardekani BA, Ashburner J, Avants B, Chiang MC, Christensen GE, Collins DL, Gee J, Hellier P, Song JH, Jenkinson M, Lepage C, Rueckert D, Thompson P, Vercauteren T, Woods RP, Mann JJ, Parsey RV. Evaluation of 14 nonlinear deformation algorithms applied to human brain MRI registration. NeuroImage. 2009; 46:786–802. [PubMed: 19195496]

Leboyer M, Bellivier F, Nosten-Bertrand M, Jouvent R, Pauls D, Mallet J. Psychiatric genetics: search for phenotypes. Trends Neurosci. 1998; 21:102–105. [PubMed: 9530915]

Lemonde S, Turecki G, Bakish D, Du L, Hrdina PD, Bown CD, Sequeira A, Kushwaha N, Morris SJ, Basak A, Ou XM, Albert PR. Impaired repression at a 5-hydroxytryptamine 1A receptor gene polymorphism associated with major depression and suicide. J Neurosci. 2003; 23:8788–8799. [PubMed: 14507979]

Mann JJ, Bortinger J, Oquendo MA, Currier D, Li S, Brent DA. Family history of suicidal behavior and mood disorders in probands with mood disorders. The American journal of psychiatry. 2005; 162:1672–1679. [PubMed: 16135627]

Mawlawi O, Martinez D, Slifstein M, Broft A, Chatterjee R, Hwang DR, Huang Y, Simpson N, Ngo K, Van Heertum R, Laruelle M. Imaging human mesolimbic dopamine transmission with positron emission tomography: I. Accuracy and precision of D(2) receptor parameter measurements in ventral striatum. Journal of cerebral blood flow and metabolism: official journal of the International Society of Cerebral Blood Flow and Metabolism. 2001; 21:1034–1057.

Milak MS, DeLorenzo C, Zanderigo F, Prabhakaran J, Kumar JS, Majo VJ, Mann JJ, Parsey RV. In vivo quantification of human serotonin 1A receptor using 11C-CUMI-101, an agonist PET radiotracer. Journal of nuclear medicine: official publication, Society of Nuclear Medicine. 2010; 51:1892–1900.

Miller JM, Brennan KG, Ogden TR, Oquendo MA, Sullivan GM, Mann JJ, Parsey RV. Elevated serotonin 1A binding in remitted major depressive disorder: evidence for a trait biological abnormality. Neuropsychopharmacology: official publication of the American College of Neuropsychopharmacology. 2009; 34:2275–2284. [PubMed: 19458612]

Ogden RT, Tarpey T. Estimation in regression models with externally estimated parameters. Biostatistics. 2006; 7:115–129. [PubMed: 16020616]

Pantazatos SP, Talati A, Pavlidis P, Hirsch J. Decoding unattended fearful faces with whole-brain correlations: an approach to identify condition-dependent large-scale functional connectivity. PLoS Comput Biol. 2012; 8:e1002441. [PubMed: 22479172]

Parsey RV, Arango V, Olvet DM, Oquendo M, Van Heertum R, Mann JJ. Regional Heterogeneity of 5-HT1A Receptors in Human Cerebellum as Assessed by Positron Emission Tomograph. Journal of Cerebral Blood Flow and Metabolism. 2005

Parsey RV, Ogden RT, Miller JM, Tin A, Hesselgrave N, Goldstein E, Mikhno A, Milak M, Zanderigo F, Sullivan GM, Oquendo MA, Mann JJ. Higher serotonin 1A binding in a second major depression cohort: modeling and reference region considerations. Biological psychiatry. 2010a; 68:170–178. [PubMed: 20497898]

Parsey RV, Ogden RT, Miller JM, Tin A, Hesselgrave N, Goldstein E, Mikhno A, Milak M, Zanderigo F, Sullivan GM, Oquendo MA, Mann JJ. Higher Serotonin 1A Binding in a Second Major Depression Cohort: Modeling and Reference Region Considerations. Biological psychiatry. 2010b

Parsey RV, Oquendo MA, Ogden RT, Olvet DM, Simpson N, Huang YY, Van Heertum RL, Arango V, Mann JJ. Altered serotonin 1A binding in major depression: a [carbonyl-C-11]WAY100635 positron emission tomography study. Biol Psychiatry. 2006; 59:106–113. [PubMed: 16154547]

Parsey, RV., Slifstein, M., Hwang, D., Abi-Dargham, A., Simpson, N., Guo, NN., Shinn, A., Mawlawi, O., Van Heertum, R., Mann, JJ., Laruelle, M. Comparison of Kinetic Modeling Methods for the In Vivo Quantification of 5-HT1A Receptors Using WAY 100635. In: Gjedde, A.Hansen, SB.Knudsen, GM., Paulson, OB., editors. Physiological Imaging of the Brain with PET. Academic Press; San Diego: 2001. p. 249-255.

Parsey RV, Slifstein M, Hwang DR, Abi-Dargham A, Simpson N, Mawlawi O, Guo NN, Van Heertum R, Mann JJ, Laruelle M. Validation and reproducibility of measurement of 5-HT1A receptor parameters with [carbonyl-11C]WAY-100635 in humans: comparison of arterial and reference tisssue input functions. Journal of cerebral blood flow and metabolism: official journal of the International Society of Cerebral Blood Flow and Metabolism. 2000; 20:1111–1133.

Peterson BS, Weissman MM. A brain-based endophenotype for major depressive disorder. Annu Rev Med. 2011; 62:461–474. [PubMed: 21226617]

Richardson-Jones JW, Craige CP, Guiard BP, Stephen A, Metzger KL, Kung HF, Gardier AM, Dranovsky A, David DJ, Beck SG, Hen R, Leonardo ED. 5-HT1A autoreceptor levels determine vulnerability to stress and response to antidepressants. Neuron. 2010; 65:40–52. [PubMed: 20152112]

Sargent PA, Kjaer KH, Bench CJ, Rabiner EA, Messa C, Meyer J, Gunn RN, Grasby PM, Cowen PJ. Brain serotonin1A receptor binding measured by positron emission tomography with [11C]WAY-100635: effects of depression and antidepressant treatment. Archives of general psychiatry. 2000; 57:174–180. [PubMed: 10665620]

Shively CA, Friedman DP, Gage HD, Bounds MC, Brown-Proctor C, Blair JB, Henderson JA, Smith MA, Buchheimer N. Behavioral depression and positron emission tomography-determined serotonin 1A receptor binding potential in cynomolgus monkeys. Archives of general psychiatry. 2006; 63:396–403. [PubMed: 16585468]

Slifstein M, Parsey RV, Laruelle M. Derivation of [(11)C]WAY-100635 binding parameters with reference tissue models: effect of violations of model assumptions. Nuclear medicine and biology. 2000; 27:487–492. [PubMed: 10962256]

Sullivan GM, Ogden RT, Oquendo MA, Kumar JS, Simpson N, Huang YY, Mann JJ, Parsey RV. Positron emission tomography quantification of serotonin-1A receptor binding in medication-free bipolar depression. Biol Psychiatry. 2009; 66:223–230. [PubMed: 19278673]

Uhl GR, Grow RW. The burden of complex genetics in brain disorders. Archives of general psychiatry. 2004; 61:223–229. [PubMed: 14993109]

Vapnik VN. An overview of statistical learning theory. IEEE transactions on neural networks/a publication of the IEEE Neural Networks Council. 1999; 10:988–999.

Wu S, Ogden RT, Mann JJ, Parsey RV. Optimal metabolite curve fitting for kinetic modeling of 11C-WAY-100635. Journal of nuclear medicine: official publication, Society of Nuclear Medicine. 2007; 48:926–931.

Zimmerman, M. Interview guide for evaluating DSM-IV psychiatric disorders and the mental status examination. Psych Products Press; 1994.

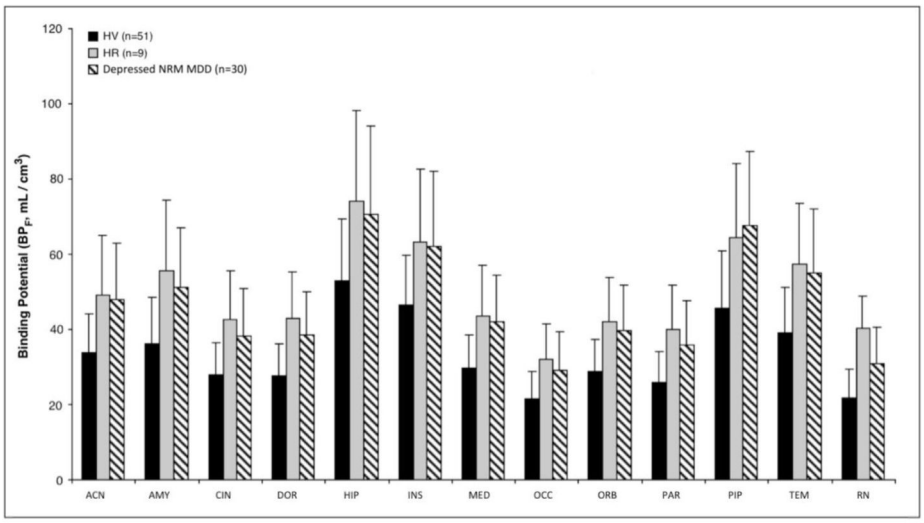

Figure 1. High Risk (HR) subjects differ significantly from Healthy Volunteer (HV) ($p = 0.004$) but do not differ from Depressed Not-Recently Medicated (NRM) Major Depressive Disorder (MDD) subjects ($p = 0.884$) across all 13 regions of interest

(anterior cingulate = ACN; amygdala = AMY; cingulate body = CIN; dorsolateral prefrontal cortex = DOR; hippocampus = HIP; insula = INS; medial prefrontal cortex = MED; occipital lobe = OCC; orbital prefrontal cortex = ORB; parietal lobe = PAR; parahippocampal gyrus = PIP; temporal lobe = TEM; raphe nuclei = RN). Figure bars represent the group mean 5-HT_{1A} BP_F weighted by bootstrap standard errors for each region, while the error bars display the corresponding weighted standard deviations.

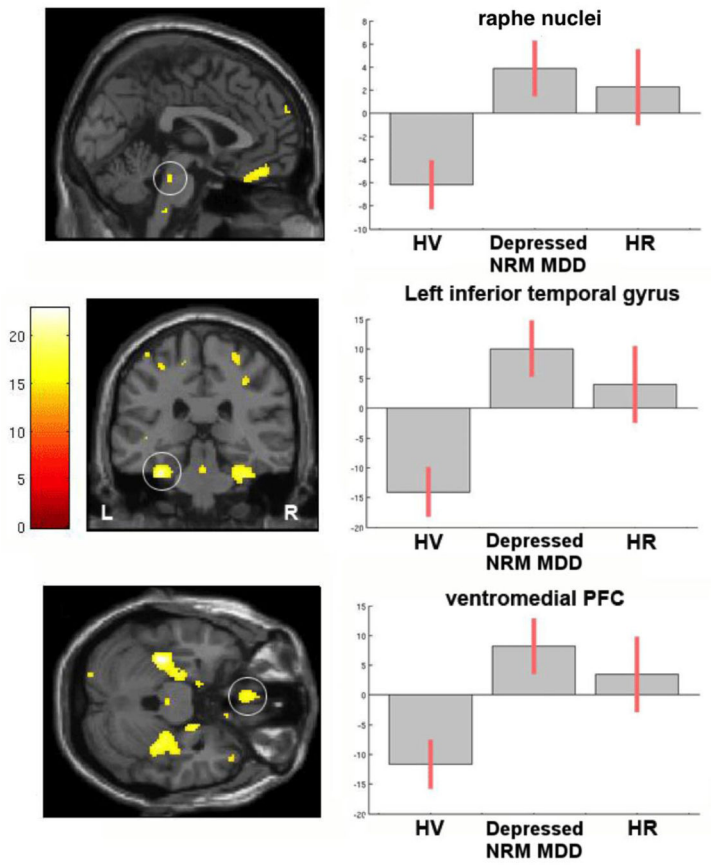

Figure 2. Voxel-based 5-HT_{1A} BP_F contrast maps for group differences across Healthy Volunteer (HV), Depressed Not-Recently Medicated (NRM) Major Depressive Disorder (MDD) and High Risk (HR) subjects (omnibus *F-test* using family-wise error rate (FWE) correction at $p < 0.05$)

Plots of average (mean-centered) BP_F values adjusted for sex in a midbrain cluster in the vicinity of dorsal raphe nucleus (top row), left inferior temporal gyrus (middle row) and ventromedial prefrontal cortex (PFC, bottom row). Statistical maps were thresholded using FWE correction at $p < 0.05$, cluster size (k) ≤ 10. Error bars represent 90% confidence intervals (CI). Supplementary Table 2 lists all regions surviving $p < 0.05$ FWE correction.

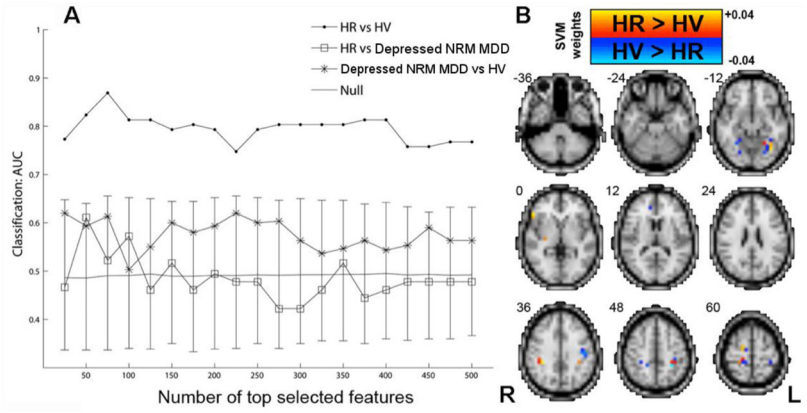

Figure 3. MVPA using whole-brain 5-HT$_{1A}$ BP$_F$ maps to classify High Risk (HR), Depressed Not-Recently Medicated (NRM) Major Depressive Disorder (MDD) and Healthy Volunteer (HV) subjects

(A) Classification performance (AUC) was plotted *vs.* number of features that have been ranked by their absolute *t-score* (in the training data). **(B)** The top 75 features (voxels) over the entire dataset were used to train a classification model and their SVM weights are displayed neuroanatomically. Informative voxels for HR *vs.* HV include fusiform and parahippocampal gyrus ($z = -12$), ventrolateral prefrontal cortex ($z = 0$), anterior cingulate ($z = 12$), inferior and superior parietal lobe ($z = 36, 48, 60$). Solid gray line represents mean for the null distribution and error bars represent 95% confidence intervals (CI) for the null distribution. Note that all HR *vs.* HV values are outside of the 95% CI. Note that due to cortical folding adjacent voxels in 3D are often actually not adjacent (i.e., they are more distal when displayed on a flattened cortical surface) (see section entitled “Supplementary Material for Figure 3”).

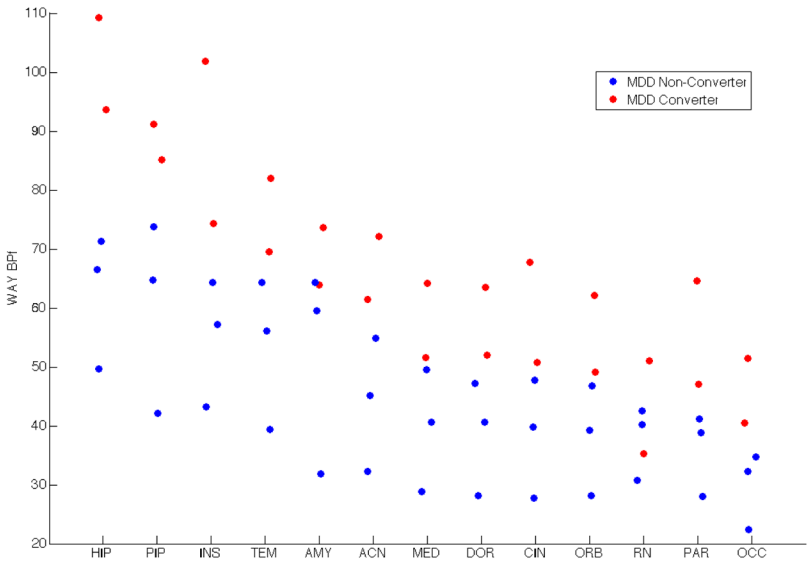

Figure 4.

High Risk (HR) subjects who converted to major depressive disorder (MDD) show higher 5-HT_{1A} BP_F systematically across regions of interest than HR subjects who did not convert to MDD (hippocampus = HIP; parahippocampal gyrus = PIP; insula = INS; temporal lobe = TEM; amygdala = AMY; anterior cingulate = ACN; medial prefrontal cortex = MED; dorsolateral prefrontal cortex = DOR; cingulate body = CIN; orbital prefrontal cortex = ORB; raphe nuclei = RN; parietal lobe = PAR; occipital lobe = OCC).

Table 1

Demographic and Clinical Features in High Risk (HR), Healthy Volunteer (HV) and Depressed Not-Recently Medicated (NRM) Major Depressive Disorder (MDD) Subjects

Table 1	**HR**	**HV**	**Depressed NRM MDD**	***p*- values**	
				HR *vs.* HV	**HR *vs.* Depressed NRM MDD**
N	9	51	30		
Age (mean ± *SD*)	25.5 ± 3.4	37.4 ± 14.5	40.6 ± 13.1	0.02	0.002
Female (*N* | %)	5 55.6%	29 56.9%	22 73.3%	0.94 *	0.27 *
Aggression (mean ± *SD*)	15.4 ± 3.3	14.90 ± 3.7	18.5 ± 5.1	0.68	0.1
HDRS (mean ± *SD*)	4 ± 2.7	0.7 ± 1.0	26.1 ± 0.4	0.006	3.7E-16

*denotes Fisher's Exact Test.

Table 2

Multivoxel Pattern Analysis (MVPA) Classification Results in High Risk (HR), Healthy Volunteer (HV) and Depressed Not-Recently Medicated (NRM) Major Depressive Disorder (MDD) Subjects (AUC = area under the receiver operating characteristic curve)

Classification	mean AUC	mean AUC *p*-value	peak AUC	sensitivity	specificity	*p*-value
Depressed NRM MDD (*N*=29) *vs.* HV (*N*=51)	0.58	0.17	0.62	0.5	0.74	0.08
HR (*N*=9) *vs.* HV (*N*=51)	0.80	< 0.005	0.87	0.78	0.96	0.00025 *
HR (*N*=9) *vs.* Depressed NRM MDD (*N*=29)	0.49	0.43	0.61	0.56	0.67	0.098

* denotes $p < 0.05$ after Bonferroni Correction.